Available online at www.sciencedirect.com
ScienceDirect
ELSEVIER
Palaeogeography, Palaeoclimatology, Palaeoecology 253 (2007) 323–331
PALAEO
www.elsevier.com/locate/palaeo

Pyrite framboids in the Permian–Triassic boundary section at Meishan, China: Evidence for dysoxic deposition

Wenjie Shen [a,b], Yangting Lin [c,*], Lin Xu [d], Jianfeng Li [e], Yasheng Wu [f], Yongge Sun [g]

[a] *Key Laboratory of Isotope Geochronology and Geochemistry, Guangzhou Institute of Geochemistry, Chinese Academy of Sciences, Guangzhou 510640, China*
[b] *Graduate School of Chinese Academy of Sciences, Beijing 100049, China*
[c] *State Key Laboratory of Lithosphereic Evolution, Institute of Geology and Geophysics, Chinese Academy of Sciences, Beijing 100029, China*
[d] *National Astronomical Observatories, Chinese Academy of Sciences, Beijing 100012, China*
[e] *Key Laboratory of Marginal Sea Geology, Guangzhou Institute of Geochemistry and South China Sea Institute of Oceanology, Chinese Academy of Sciences, Guangzhou 510640, China*
[f] *Division of Water Resource and Crust Fluid, Institute of Geology and Geophysics, Chinese Academy of Sciences, Beijing 100029, China*
[g] *The State Key Laboratory of Organic Geochemistry, Guangzhou Institute of Geochemistry, Chinese Academy of Sciences, Guangzhou 510640, China*

Received 6 January 2007; received in revised form 6 June 2007; accepted 6 June 2007

Abstract

Pyrite framboid evidence from the Permian–Triassic global stratotype at Meishan, China, indicates the late Permian mass extinction is closely associated with a dramatic decline of benthic oxygen levels. Sizes and abundances of the framboids were determined from acid residues and in situ on polished sections of the samples. The framboids are abundant in the thin pyrite lamina on the top of Bed 24e (the upper layer of Bed 24), and Beds 25, 26 and 29, rare in Bed 24e and Bed 28, but absent in Bed 27. They have narrow size distributions with average diameters from 4.6 μm to 8.7 μm which are similar to those formed under anoxic/dysoxic conditions. The abundances and mean diameters of the pyrite framboids indicate redox conditions of deposition changing from upper dysoxia (Bed 24e) and lower dysoxia (pyrite lamina, Beds 25 and 26) to oxygenation (Bed 27), and again to upper dysoxia (Bed 28) and lower dysoxia (Bed 29). Our discovery confirms a worldwide dysoxic marine event during the Permian–Triassic transition, suggestive of a direct relationship with the Permian–Triassic marine mass extinction.

Keywords: Permian–Triassic boundary; Pyrite framboid; Dysoxia; Mass extinction

1. Introduction

The mass extinction of the Permian–Triassic boundary (hereafter PTB) is one of the most severe events in the Earth's evolutionary history. However, causes of the event are a long-standing controversial issue (Erwin, 1993; Erwin et al., 2002). Massive volcanic eruptions (Campbell et al., 1992; Yin et al., 1992, 2007; Renne et al., 1995; Bowring et al., 1998; Courtillot et al., 1999; Lo et al., 2002; Kamo et al., 2003; Grard et al., 2005), bolide impacts (Xu and Yan, 1993; Retallack et al., 1998; Becker et al., 2001; Kaiho et al., 2001; Basu et al., 2003; Becker, 2004), or coincidence of them (Zhou et al., 1991; Chai et al., 1992; Jin et al., 2000) were proposed to explain the global changes of the

* Corresponding author. Tel.: +86 10 62007112.
E-mail address: Linyt@mail.iggcas.ac.cn (Y. Lin).

0031-0182/$ - see front matter © 2007 Elsevier B.V. All rights reserved.
doi:10.1016/j.palaeo.2007.06.005

ecosystem. One of the possible catastrophic changes was marine anoxia (Wignall and Twitchett, 1996; Isozaki, 1997; Grice et al., 2005; Wignall et al., 2005). A line of evidence for the marine anoxia is common or abundant pyrite framboids in the sections, which are spherical aggregates of pyrite microcrystals and similar to those in modern/ancient marine sediments formed under oxygen-restricted conditions (Wilkin et al., 1996, 1997; Wignall and Newton, 1998). The occurrence and morphology of pyrite framboids are sensitive to the redox conditions. Euxinic pyrite framboids usually form at depths close to the redox boundary, and they rarely exceed 6 μm in diameter before sinking to the seafloor. Secondary growth of the framboids is limited in anoxic environments (O_2-free). Thus, a narrow size distribution of pyrite framboids indicates euxinic conditions (H_2S-bearing, O_2-free bottom waters) (Bond et al., 2004; Racki et al., 2004). Other morphologies of pyrite, including large euhedral crystals and amorphous lumps, have no obvious correlation with oxygen-restricted biofacies (Wignall and Newton, 1998).

Pyrite framboids were reported as key evidence of anoxia in the PTB sections at eastern Greenland (Wignall and Twitchett, 2002), southwestern Japan (Isozaki, 1997), Sosio valley (Wignall and Twitchett, 2002), Italy (Wignall and Twitchett, 1996), Slovenia (Wignall and Twitchett, 1996), and Kashmir (Wignall et al., 2005). The PTB section at Meishan, China, is referred to as the Global Stratotype Section and Point (GSSP) of the Permian–Triassic Boundary (Yin et al., 2001, 2005). However, no pyrite framboids were hitherto reported in the Meishan PTB event layer (the pyrite lamina) or in the layers of clay (Bed 25) and mudstone (Bed 26). Jin et al. (2000) found some pyrite framboids only in the overlying (Bed 29) and underlying (Bed 24) beds of the Meishan PTB section, and they suggested that the severe mass extinction recorded in Bed 25 was not related to marine anoxia. However, Wignall and Twitchett (2002) suggested anoxic conditions of the Meishan PTB section. Jiang et al.(2006) measured contents and sulfur isotopic compositions of pyrite near PTB in Meishan section. However, they didn't notice pyrite framboids. In this paper, we report the first discovery of pyrite framboids in the pyrite lamina and in Beds 25 and 26 at Meishan PTB section, and discuss the depositional conditions and the relationship with the PTB mass extinction event.

2. Samples and experiments

Samples were collected from Bed 24e to Bed 29 at the quarry C, Meishan section (Fig. 1). The PTB, defined by the first appearance of *Hindeodus parvus*, occurs at the base of Bed 27c (Yin et al., 2001, 2005). The pyrite lamina (about 3 mm) on the top of Bed 24e was referred to as the event-stratigraphic boundary (Jin et al., 2000; Li et al., 2005; Shen et al., 2006).

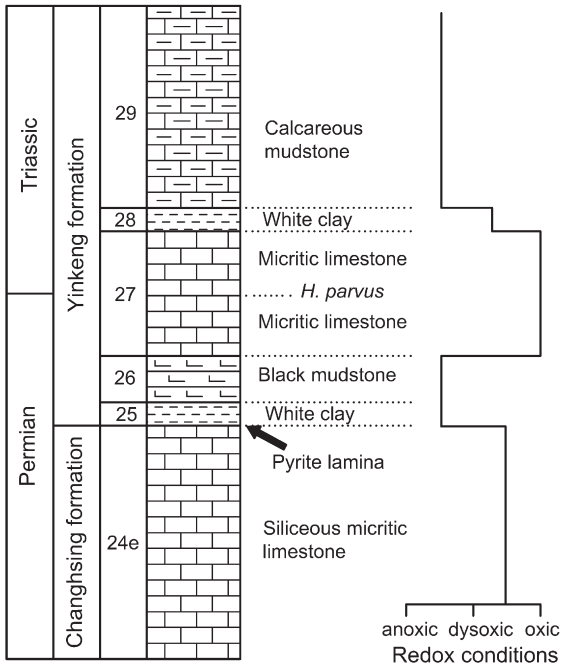

Fig. 1. The strata sequence of the Meishan PTB section, plotted with redox conditions indicated by the size distributions of the pyrite framboids. The main mass extinction event occurs at the pyrite lamina, which coincides with the drop of oxygen levels.

Two or three polished blocks of each bed were made for in situ observation of pyrite framboids. The samples were embedded in epoxy, and then ground and polished with oil in order to avoid swelling of the mudstone and clay in water. In addition, another set of samples, i.e. about 40 g each from Beds 25 and 26, and about 5 g each from Beds 24, 27, 28 and 29, were etched first with 3 M HCl to dissolve carbonate and then with 10 M HF/1 M HCl to destroy silicates. The acid residues were washed with distilled water for three times, and then aliquots of the residues were deposited on glass slides for observation.

Both polished blocks and acid residues were observed with a FEI Quanta 400 scanning electron microscope (SEM) equipped with a GENESRS 2000 energy dispersive spectrometer (EDS) in the Key Laboratory of Marginal Sea Geology, Guangzhou Institute of Geochemistry and South China Sea Institute of Oceanology, Chinese Academy of Sciences. The

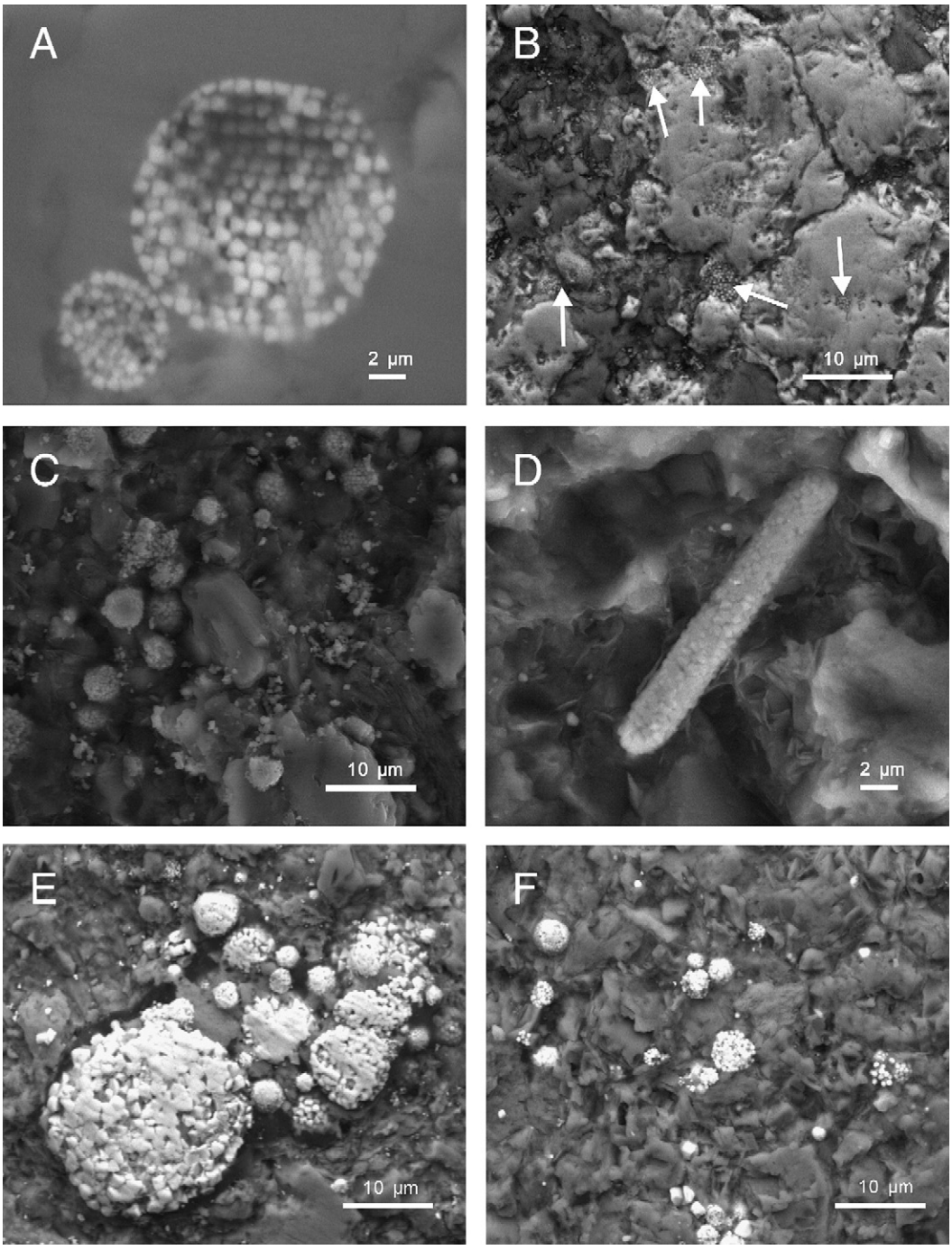

Fig. 2. In situ occurrences of pyrite framboids from the Meishan PTB section. (A) Pyrite framboids in Bed 24e, showing the spheroidal assemblages of submicron-sized crystals of pyrite. Backscattered electron image with a scale bar of 2 μm; (B) Pyrite framboids (arrows) enclosed within lumps of pyrite in the pyrite lamina. Backscattered electron image with a scale bar of 10 μm; (C) Abundant pyrite framboids in Bed 26. Secondary electron image with a scale bar of 10 μm; (D) A tube-like pyrite framboid in Bed 26. Secondary electron image with a scale bar of 2 μm; (E) Pyrite framboids in Bed 26, one has an unusually large size. Backscattered electron image with a scale bar of 10 μm; (F) Pyrite framboids in Bed 29. Backscattered electron image with a scale bar of 10 μm.

accelerating voltage is 20 kV, and spatial resolution of the secondary electron image is better than 3 nm. Statistical counting and measurement of pyrite framboids were performed on the images, using photographical software XT DOCU. The measured apparent diameters of pyrite framboids are smaller than the true values, but the deviation is less than 10% (Wilkin et al., 1996; Wignall and Newton, 1998).

3. Results

3.1. Pyrite framboids observed in situ

Pyrite framboids are spheroidal to sub-spheroidal assemblages composed of sub-micron crystals of pyrite (Fig. 2). Other occurrences of pyrite are cubic crystals and irregular lumps. The framboids were abundant in the pyrite lamina and in Beds 26 and 29, rare in Beds 24e and 25, and absent in Beds 27 and 28 (Table 1).

3.1.1. Bed 24e

Only 8 framboids were observed in a 1.2 cm^2 area of the polished block. Most of the framboids are 4–5 μm in diameter, with a maximum of 12.2 μm (Fig. 2A).

3.1.2. Pyrite lamina

Pyrite framboids are common, mainly interstitial to or enclosed in the pyrite lumps (Fig. 2B). The sharp boundaries between the framboids and pyrite lumps indicate that the morphology of the framboids was little modified during diagenesis. The mean diameter of the framboids is (1σ) 5.4±1.7 μm.

Table 1
Statistics of pyrite framboids in the sediments of the Meishan PTB section

Strata	Framboid content (number per mm^2)	Framboids size [a] (μm)	Depositional conditions [b]
Bed 29	517	5.0±2.8 (n=46)	Lower dysoxic
Bed 28 [c]	–	8.7±2.0 (n=24)	Upper dysoxic
Bed 27	–	No framboid	Oxic
Bed 26	945	4.6±3.5 (n=104)	Lower dysoxic
Bed 25 [c]	–	6.0±2.7 (n=89)	Lower dysoxic
Pyrite lamina	180	5.4±1.7 (n=27)	Lower dysoxic
Bed 24e	7	Rare	Upper dysoxic

[a] Mean diameter±1σ, in parentheses is the statistic numbers.
[b] After the definition of Bond et al. (2004) and Racki et al. (2004).
[c] Acid etched samples.

3.1.3. Bed 25

Only 5 framboids were observed in the polished block. The largest one has a diameter of about 10 μm, and the other four are within 2–5 μm in diameter. It is possible that most framboids were lost during polishing process because of the very soft surface of clay. A large number of the framboids were found in the etched residue of the sample (see the next subsection).

3.1.4. Bed 26

Framboids are abundant (945 per mm^2). Most of the framboids occur as clusters (Fig. 2C and E), and some of them are interstitial to the clumps of pyrite. The framboids show no genetic relationship with the clumps of pyrite. The mean diameter of the framboids is (1σ) 4.6±3.5 μm, slightly smaller than that of those in the pyrite lamina, but with a larger standard deviation than the latter. A few of the framboids are overgrown, with sizes up to 30 μm. In addition, there are a few of tube-like framboids (2.7×17.7 μm) (Fig. 2D), which were probably formed by different kinds of microorganism.

3.1.5. Beds 27 and 28

No pyrite framboid was found.

3.1.6. Bed 29

The pyrite framboids are abundant (517 per mm^2), and occur as single assemblages (Fig. 2F). The mean diameter is (1σ) 5.0±2.8 μm.

3.2. Pyrite framboids in the etched residues

As described above, abundant framboids were found in situ in the pyrite lamina and in Beds 26 and 29. In contrast, only a few grains were observed in Bed 25 and none in Bed 28. The low abundance of framboids in Bed 25 and their absence in Bed 28 are inconsistent with previous estimation of anoxic conditions (Wignall and Twitchett, 2002). In order to reconfirm the in situ results, the other set of the samples were etched with HCl and HF, and the residues were observed with SEM. The residues consist predominantly of pyrite, and the abundances of the residues are 0.28% (Bed 24e), 1.70% (Bed 25), 4.65% (Bed 26), 1.33% (Bed 27), 5.03% (Bed 28) and 1.60% (Bed 29), respectively.

3.2.1. Bed 24e

Pyrite is extremely small in size (<1 μm). No framboid of pyrite was found.

3.2.2. Bed 25

The residue consists predominantly of pyrite (Fig. 3A), with ~40 vol.% as framboids, ~50 vol.% as euhedral crystals and 10 vol.% as irregular lumps. The diameters of the framboids rang from 2.4 μm to 16.7 μm with a mean value of (1σ) 6.0±2.7 μm.

3.2.3. Bed 26

The acid residues of Bed 26 are nearly pure pyrite, and the predominant grains (>90%) are framboids with a few of cubic crystals (Fig. 3B). The framboids are similar to those observed in situ described above. Measurement of 135 framboids gives a mean diameter of (1σ) 5.2±2.8 μm, which is slightly larger than the in situ observation (4.6±3.5 μm). Tube-like framboids of pyrite were also found in the residues, similar to those observed in situ.

3.2.4. Bed 27

No framboids were found in the etched residue, confirming the absence of the framboids in the polished block.

3.2.5. Bed 28

The etched residue contains very low abundance of the framboids, with only 24 assemblages (Fig. 3C) observed in an area of 0.25 mm^2. This is consistent with the failure of in situ discovery of the framboids. The sizes of the framboids range from 4.3 μm to 11.8 μm with a larger mean diameter (8.7±2.0 μm) in comparison with those in other beds.

3.2.6. Bed 29

The framboids are common in the etched residue, usually smaller than 6 μm in diameter (Fig. 3D).

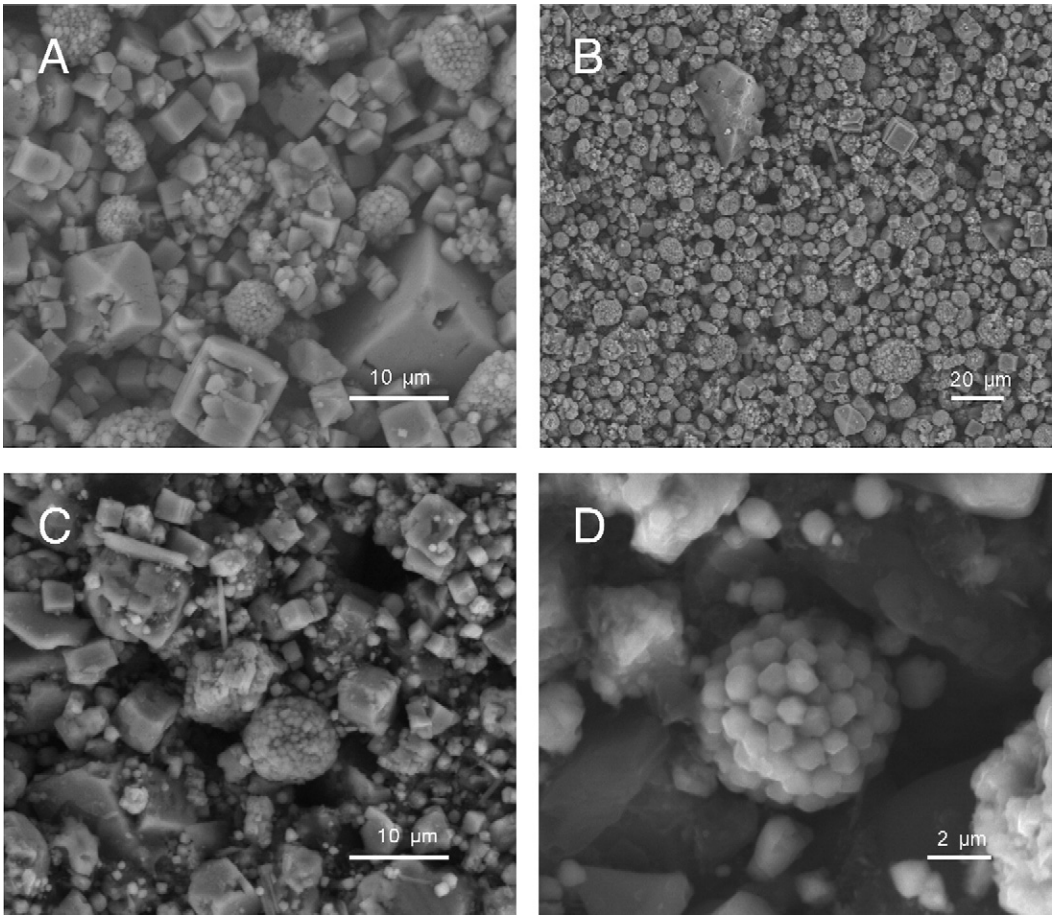

Fig. 3. Secondary electron images of pyrite framboids in the HCl–HF etched residues from the Meishan PTB section. (A) The residue of Bed 25, consisting of nearly pure pyrite with about 40% as framboids. The scale bar is 10 μm; (B) The residue of Bed 26, consisting of predominant pyrite framboids with a few cubic or irregular grains of pyrite. The scale bar is 10 μm; (C) The acid residue of Bed 28, consisting mainly of cubic and framboidal pyrite. The scale bar is 10 μm; (D) A pyrite framboid with diameter of about 6 μm in the residue of Bed 29. The scale bar is 2 μm.

4. Discussion

Based on chalcophile elements, color and lamina of sediment, bioturbation and occurrence of pyrite (but not in the form of framboids), Wignall and Twitchett (2002) suggested a variation sequence of the redox condition in the Meishan PTB section, from oxygenation (Bed 24e), anoxia (pyrite lamina), anoxia (Bed 25), progressive oxygenation (Bed 26), oxygenation (Bed 27), anoxia (Bed 28), and to oxygenation (Bed 29). However, Erwin et al. (2002) criticized that the laminated sediments and the absence of active bioturbation may have reflected not a condition of anoxia, but the mass extinction. In addition, part of the pyrite was formed during diagenesis. Jin et al. (2000) found no pyrite framboids in Bed 25, 26 or 28, and concluded that there was no any anoxic event contemporary with the mass extinction at Meishan section. Jiang et al. (2006) determined the contents and sulfur isotopic compositions of pyrite near the

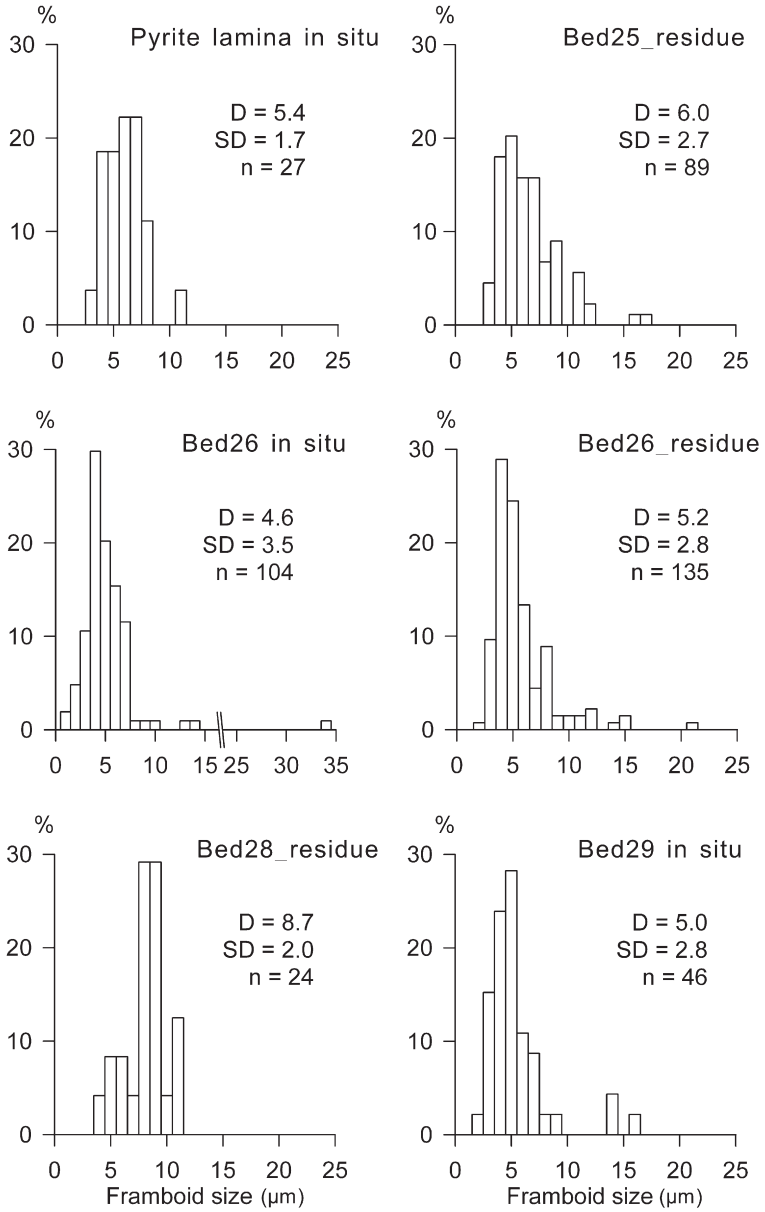

Fig. 4. Size distributions of the pyrite framboids in the Meishan PTB section. D = mean diameter of the framboids (μm); SD = standard deviation of the measurements; n = numbers.

PTB in Meishan section, but they didn't report any pyrite framboids.

Our discovery of pyrite framboids renews the studies in Meishan PTB section. The occurrence of pyrite framboids in the Meishan PTB section and their size distributions (small mean diameters of 4.6–8.7 μm, and the standard deviations of 1.7–3.5 μm) are similar to those reported in modern/ancient marine sediments formed under anoxic/dysoxic conditions (Wilkin et al., 1996, 1997; Wignall and Twitchett, 2002; Wignall et al., 2005), suggestive of dysoxic conditions in the location of Meishan during the PTB period. Similar pyrite framboids were reported in several other PTB sections in eastern Greenland (Wignall and Twitchett, 2002), southwestern Japan (Isozaki, 1997), Sosio valley (Wignall and Twitchett, 2002), Italy (Wignall and Twitchett, 1996), Slovenia (Wignall and Twitchett, 1996), and Kashmir (Wignall et al., 2005), and they were referred to as an indicator of oxygen-poor depositional conditions.

Bond et al. (2004) and Racki et al. (2004) pointed out abundant and small framboids (<5 μm), probably with rare larger assemblages, are indicative of lower dysoxic deposition; common or rare framboids with a broad size range are indicative of upper dysoxic deposition; absence of framboids is indicative of oxic deposition. Lower and upper dysoxia represent two different extents of oxygen deficiency, and the former is more serious. Thus, oxygen level of each bed in Meishan section can be determined accordingly. Bed 26 and 29 have abundant small framboids, but with a broad size range of framboids (standard deviation >2 μm, Table 1; Fig. 4) and intense bioturbation (Wignall and Twitchett, 2002). Their depositional conditions are referred to as lower dysoxia. The framboids in Bed 25 and the pyrite lamina are slightly bigger, but still less than 6 μm (Table 1; Fig. 4), indicative of lower dysoxic depositions too. In contrast, the average diameter of framboids in Bed 28 is significantly larger than 6 μm, and the framboids in Bed 24e are rare, suggestive of upper dysoxic deposition (Table 1; Fig. 4).

According to the abundances and size distributions of the pyrite framboids in the Meishan PTB section, we suggest a sequence of the redox conditions as below: upper dysoxia (Bed 24e), lower dysoxia (pyrite lamina), lower dysoxia (Bed 25), lower dysoxia (Bed 26), oxygenation (Bed 27), upper dysoxia (Bed 28), and lower dysoxia (Bed 29) (Fig. 1; Table 1). It is noticed that dysoxic conditions were prevailing during the PTB event at the Meishan section. The white clay of Bed 25 and pyrite lamina are volcanogenic. Based on the contents of pyrite and its sulfur isotopic compositions of the Meishan PTB samples, Jiang et al. (2006) suggested that a large volume of H_2S from volcanoes probably added into ocean and caused the water poisonous and oxygen-poor. The black, organic-rich mudstone of Bed 26 indicates a relative surplus of primary productivity (Fang, 2004; Xie et al., 2005; Wang, 2007). The abundant small pyrite framboids in Bed 26 were likely formed due to intensive activity of sulphate reducing bacteria (Fang, 2004).

The sequence of redox conditions indicated by the pyrite framboids in the Meishan PTB section is generally consistent with that proposed by Wignall and Twitchett (2002). Our new data confirm a worldwide oxygen-poor marine setting during the PTB event, which could be related with the marine mass extinction (Wignall and Twitchett, 1996; Isozaki, 1997; Grice et al., 2005; Wignall et al., 2005; Wang, 2007; Xie et al., 2007). The marine dysoxia, together with the terrestrial oxygen deficiency (Huey and Ward, 2005), is probably provoked by the intensive volcanism.

5. Conclusions

Pyrite framboids were at the first time found in the pyrite lamina on the top of Bed 24e and in Beds 25, 26, 28 and 29 in the Meishan PTB section. The size and abundance distributions of the pyrite framboids indicate dysoxic deposition that coincides with the mass extinction event. The discovery of pyrite framboids in the Meishan section confirms a worldwide oxygen-poor marine setting during the PTB period (Wignall and Twitchett, 2002), suggestive of a genetic relationship with the PTB marine biotic crisis.

Acknowledgements

The authors are thankful to Yugan Jin and Hua Zhang for providing a part of the samples from the Meishan PTB section. The helpful discussion with Yongzhang Zhou and the constructive comments by two anonymous reviewers and the editor Finn Surlyk significantly improved this paper. This study was supported by the Knowledge Innovation Program (kzcx2-yw-110) and One-Hundred-Talent Program of Chinese Academy of Sciences and by the National Natural Science Foundation of China (Grant No. 40232026).

References

Basu, A.R., Petaev, M.I., Poreda, R.J., Jacobsen, S.B., Becker, L., 2003. Chondritic meteorite fragments associated with the Permian–Triassic boundary in Antarctica. Science 302 (5649), 1388–1392.

Becker, L., 2004. A possible end-Permian impact crater offshore of northwestern Australia. Science 304, 1469–1476.

Becker, L., Poreda, R.J., Hunt, A.G., Bunch, T.E., Rampino, M., 2001. Impact event at the Permian–Triassic boundary: evidence from extraterrestrial noble gases in fullerenes. Science 291, 1530–1534.

Bond, D., Wignall, P.B., Racki, G., 2004. Extent and duration of marine anoxia during the Frasnian–Famennian (Late Devonian) mass extinction in Poland, Germany, Austria and France. Geological Magazine 141 (2), 173–193.

Bowring, S.A., Erwin, D.H., Jin, Y.G., Martin, M.W., Davidek, K., Wang, W., 1998. U/Pb zircon geochronology and tempo of the end-Permian mass extinction. Science 280 (5366), 1039–1045.

Campbell, I.H., Czamanske, G.K., Fedorenko, V.A., Hill, R.I., Stepanov, V., 1992. Synchronism of the Siberian traps and the Permian–Triassic boundary. Science 258, 1760–1763.

Chai, C., Zhou, Y., Mao, X., Ma, S., Ma, J., Kong, P., He, J., 1992. Geochemical constraints on the Permo-Triassic boundary event in South China. In: Sweet, W.C., Yang, Z., Dickins, J.M., Yin, H. (Eds.), Permo-Triassic Events in the Eastern Tethys, Stratigraphy, Classification, and Relations with the Western Tethys. Cambridge University Press, pp. 158–168.

Courtillot, V., Jaupart, C., Manighetti, I., Tapponnier, P., Besse, J., 1999. On causal links between flood basalts and continental breakup. Earth and Planetary Science Letters 166 (3–4), 177–195.

Erwin, D.H., 1993. The great Paleozoic crisis. Columbia University Press, New York.

Erwin, D.H., Bowring, S.A., Yugan, J., 2002. End-Permian mass extinctions: a review. In: Koebel, C., MacLeod, K.G. (Eds.), Catastrophic Events and Mass Extinctions: Impacts and Beyond: Boulder, Colorado. Geological Society of America Special Paper, vol. 356, pp. 363–383.

Fang, Z., 2004. The Permian–Triassic boundary crisis: patterns of extinction, collapse of various ecosystems, and their causes. In: Rung Jay, Fang Zingier, (Eds.), Mass extinction and recovery-evidences from the Palaeozoic and Triassic of south China. Hefei: University of Science and Technology of China Press, pp. 785–928, 1075–1076.

Grard, A., Francois, L.M., Dessert, C., Dupre, B., Godderis, Y., 2005. Basaltic volcanism and mass extinction at the Permo-Triassic boundary: environmental impact and modeling of the global carbon cycle. Earth and Planetary Science Letters 234 (1–2), 207–221.

Grice, K., Cao, C., Love, G.D., Bottcher, M.E., Twitchett, R.J., Grosjean, E., Summons, R.E., Turgeon, S.C., Dunning, W., Jin, Y., 2005. Photic zone euxinia during the Permian–Triassic superanoxic event. Science 307 (5710), 706–709.

Huey, R.B., Ward, P.D., 2005. Hypoxia, global warming, and terrestrial late Permian extinctions. Science 308 (5720), 398–401.

Isozaki, Y., 1997. Triassic boundary superanoxia and stratified superocean: records from lost deep sea. Science 276 (5310), 235–238.

Jiang, Y., Tang, Y., Dai, S., Zou, X., Qian, H., Zhou, G., 2006. Pyrites and sulfur isotopic composition near the Permian–Triassic boundary in Meishan. Zhejiang Acta Geological Sinica 80 (8), 1202–1207.

Jin, Y.G., Wang, Y., Wang, W., Shang, Q.H., Cao, C.Q., Erwin, D.H., 2000. Pattern of marine mass extinction near the Permian–Triassic boundary in South China. Science 289 (5478), 432–436.

Kaiho, K., Kajiwara, Y., Nakano, T., Miura, Y., Kawahata, H., Tazaki, K., Ueshima, M., Chen, Z., Shi, G.R., 2001. End-Permian catastrophe by a bolide impact: evidence of a gigantic release of sulfur from the mantle. Geology 29 (9), 815–818.

Kamo, S.L., Czamanske, G.K., Amelin, Y., Fedorenko, V.A., Davis, D.W., Trofimov, V.R., 2003. Rapid eruption of Siberian flood-volcanic rocks and evidence for coincidence with the Permian–Triassic boundary and mass extinction at 251 Ma. Earth and Planetary Science Letters 214 (1–2), 75–91.

Li, Y., Liang, H., Yin, H., Sun, J., Cai, H.a., Zhu, R., Ran, F., 2005. Determination of fullerenes (C_{60}/C_{70}) from the Permian–Triassic boundary in the Meishan section of south China. Acta Geologica Sinica 79 (1), 11–15.

Lo, C.-H., Chung, S.-L., Lee, T.-Y., Wu, G., 2002. Age of the Emeishan flood magmatism and relations to Permian–Triassic boundary events. Earth and Planetary Science Letters 198 (3–4), 449–458.

Racki, G., Piechota, A., Bond, D., Wignall, P.B., 2004. Geochemical and ecological aspects of lower Frasnian pyrite-ammonoid level at Kostomłoty (Holy Cross Mountains, Poland). Geological Quarterly 48 (3), 267–282.

Renne, P.R., Zichao, Z., Richards, M.A., Black, M.T., Basu, A.R., 1995. Synchrony and causal relations between Permian–Triassic boundary crises and Siberian flood volcanism. Science 269, 1413–1416.

Retallack, G.J., Seyedolali, A., Krull, E.S., Holser, W.T., Ambers, C.P., Kyte, F.T., 1998. Search for evidence of impact at the Permian–Triassic boundary in Antarctica and Australia. Geology 26 (11), 979–982.

Shen, W., Lin, Y., Wang, D., Zhou, Y., Miao, B., 2006. Advances in study of natural fullerenes with special discussion on P–T boundary fullerenes. Advances in Earth Science 21 (9), 903–910.

Wang, C., 2007. Anomalous hopane distributions at the Permian–Triassic boundary, Meishan, China — evidence for the end-Permian marine ecosystem collapse. Organic Geochemistry 38 (1), 52–66.

Wignall, P.B., Newton, R., 1998. Pyrite framboid diameter as a measure of oxygen deficiency in ancient mudrocks. American Journal of Science 298, 537–552.

Wignall, P.B., Twitchett, R.J., 1996. Oceanic anoxia and the end Permian mass extinction. Science 272, 1155–1158.

Wignall, P.B., Twitchett, R.J., 2002. Extent, duration, and nature of the Permian–Triassic superanoxic event. In: Koebel, C., MacLeod, K.G. (Eds.), Catastrophic Events and Mass Extinctions: Impacts and Beyond: Boulder, Colorado. Geological Society of America Special Paper, vol. 356, pp. 395–413.

Wignall, P.B., Newton, R., Brookfield, M.E., 2005. Pyrite framboid evidence for oxygen-poor deposition during the Permian–Triassic crisis in Kashmir. Palaeogeography, Palaeoclimatology, Palaeoecology 216 (3–4), 183–188.

Wilkin, R.T., Arthur, M.A., Dean, W.E., 1997. History of water-column anoxia in the Black Sea indicated by pyrite framboid size distributions. Earth and Planetary Science Letters 148 (3–4), 517–525.

Wilkin, R.T., Barnes, H.L., Brantley, S.L., 1996. The size distribution of framboidal pyrite in modern sediments: an indicator of redox conditions. Geochimica et Cosmochimica Acta 60 (20), 3897–3912.

Xie, S., Pancost, R.D., Yin, H., Wang, H., Evershed, R.P., 2005. Two episodes of microbial change coupled with Permo/Triassic faunal mass extinction. Nature 434 (7032), 494–497.

Xie, S., Pancost, R.D., Huang, X., Jiao, D., Lu, L., Huang, J., Yang, F., Evershed, R.P., 2007. Molecular and isotopic evidence for episodic environmental change across the Permo/Triassic boundary at Meishan in South China. Global and Planetary Change 55 (1–3), 56–65.

Xu, D.Y., Yan, Z., 1993. Carbon isotope and iridium event markers near the Permian/Triassic boundary in the Meishan section. Palaeogeography, Palaeoclimatology, Palaeoecology 104, 171–176.

Yin, H., Huang, S., Zhang, K., Hansen, H.J., Yang, F., Ding, M., Bi, X., 1992. The effects of volcanism on the Permo-Triassic mass extinction

in South China. In: Sweet, W.C., Yang, Z., Dickins, J.M., Yin, H. (Eds.), Permo-Triassic events in the eastern Tethys, stratigraphy, classification, and relations with the western Tethys. Cambridge University Press, pp. 146–157.

Yin, H., Zhang, K., Tong, J., Yang, Z., Wu, S., 2001. The global stratotype section and point of the Permian–Triassic boundary (GSSP). Episodes 24 (2), 102–114.

Yin, H., Tong, J., Zhang, K., 2005. A review on the global stratotype section and point of the Permian–Triassic boundary. Acta Geologica Sinica 79 (6), 715–728.

Yin, H., Feng, Q., Lai, X., Baud, A., Tong, J., 2007. The protracted Permo-Triassic crisis and multi-episode extinction around the Permian–Triassic boundary. Global and Planetary Change 55 (1–3), 1–20.

Zhou, Y., Chai, Z., Mao, X., Ma, S., Ma, J., Kong, P., He, J., 1991. A mixing model — the elemental geochemistry of Permian–Triassic boundaries in south China and its implications. Geological Review 37 (1), 52–63.